RSC Advances

ROYAL SOCIETY OF CHEMISTRY

www.rsc.org/advances

Cite this: DOI: 10.1039/c0xx00000x

www.rsc.org/xxxxxx

ARTICLE TYPE

Efficient Dye-Sensitized Solar Cell with Pure Thin Film of Hybrid Polyoxometalate Covalently Attached Organic Dye as a Working Electrode, in Cobalt Redox Mediator System

Davud Karimian,[a] Bahram Yadollahi, *[a] Mahmoud Zendehdel,*[a] and Valiollah Mirkhani[a]

Received (in XXX, XXX) XthXXXXXXXXX 20XX, Accepted Xth XXXXXXXXX 20XX
DOI: 10.1039/b000000x

Polyoxometalates (POMs) are a class of inorganic metal-oxygen clusters comprised of abundant element, representing unique structures and molecular weight, which possess the similar energy band structures with metal oxides. In this research, for the first time, a Keggin-type hybrid polyoxometalate $[SiW_{11}O_{39}(Si(CH_2)_3NH_2)_2O]$ (Hybrid-POM) is used as a pure semiconductor thin film in the working electrode of an efficient dye-sensitized solar cell (DSC) which fabricated by D35 organic dye as a sensitizer and one-electron fast redox mediator cobalt complex. D35 dye is attached on the surface of the POM by strong amide bond (D35@Hybrid-POM). For evaluated comparison, two DSCs also fabricated by mesoporous anatase TiO_2, with and without titania blocking layer, in the same conditions of electrolyte, sensitizer and counter electrode. J-V measurements of the DSCs was prepared under AM1.5G irradiation and photoelectrochemical parameters like open-circuit voltage (V_{oc}), short-circuit current density (J_{sc}), fill factor (FF), voltage decay and the overall efficiency measured and compared to the mesoporous titania cells. The J-V curves show promising enhancement of the overall in the DSC with D35@Hybrid-POM structure in compare with other prevalent mesoporous titania cells. Incident photon to current conversion efficiency spectra of the DSCs with D35@Hybrid-POM and mesoporous titania with TBL working electrodes, also evaluated. A maximum IPCE of about 91% found for DSC employing D35@Hybrid-POM which is about 30% higher than the DSC with mesoporous titania layer. Voltage decay measurement, calculated electron life time and effective recombination order (β) showed that the electron lifetime becomes promising longer when we use Hybrid-POM structure in the photoanode. Thus, these results show that the rate of recombination electron transfer of cobalt mediator system at the surface of Hybrid-POM is very slow.

Keywords: Dye-sensitized Solar Cell, Polyoxometalate, Hybrid Material, Cobalt Mediator, Conjugation.

1. Introduction

Polyoxometalates (POMs) are a nano-size class of Metal-Oxygen clusters, which have attracted lots of attention in the last decades. These interesting materials have been widely used in various fields such as catalysis, medicine, material sciences and analytical chemistry [1-4]. This class of inorganic compounds have found these applicabilities not only because of their versatile structures, but also in terms of redox properties, charge distribution, structure tunability and variety of shapes and distribution [5,6]. Among these fascinating properties, the photophysical and photochemical ones have received considerable attention [7-9].

[a]Department of Chemistry, University of Isfahan, Isfahan 81746-73441, Iran.
* Corresponding authors:
Mahmoud Zendehdel
Tel.: +98-31-37932748, Fax: +98-31-37932700, E-mail: m.zendehdel@sci.ui.ac.ir
BahramYadollahi
Tel.: +98-31-37932742, E-mail: yadollahi@chem.ui.ac.ir

POMs can reversibly accept and transfer electrons without changing in structure, which makes them as interesting material in the photonic and photovoltaic applications [10, 11].

One of the outstanding POMs properties is changeable photoelectric traits, which would be adjustable with changing in structure and composition [3]. POMs can accept electrons and play an electron donor role after reduction and because of this, they have been widely used in photovoltaic cells [12-14].

The dye-sensitized solar cells (DSCs) are a promising option to

conventional inorganic semiconductor-based solar cells because of environmental friendly and inexpensive materials, and fabrication [15-17]. In typical DSCs, a mesoporous film of titania nanocrystals is sensitized with organic or metal organic dyes which in most applications are surrounded by a redox mediator in an organic solvent, typically acetonitrile [18-20]. In a DSC, hole (h+) transport is accomplished by a solution phase redox mediator, which permeates the pores of the semiconductor and serves to electrically connection of the anode and cathode. A redox mediator, which displays selective heterogeneous electron transfer kinetics that rapid reduction of the oxidized mediator could be occurs only at the cathode, could minimize Electron/hole recombination. In a particularly interesting report, DSCs using the easy-to-prepare cobalt(III/II) tris(4,4′-di-*tert*-butyl-2,2′-bipyridyl), $[Co(t\text{-}Bu_2bpy)_3]^{3+/2+}$, as a redox shuttle exhibited excellent efficiencies with incident photon to current efficiencies (IPCEs) ~80% of a comparable cell employing I_3^-/I^- [21]. Several promising results have been obtained using Co(II)/Co(III) redox mediators with organic dyes and different semiconductor systems as photoanode [22-24].

In most of the fabricated dye-sensitised solar cells (DSCs) based on POMs, the POM is added in order to modify the efficiency of injection. Using POM in combination with TiO_2, ZnO or other metal-oxides, can reduce the recombination in the cells. In all of these composites, the presence of metal-oxides is necessary to be utilized as an under-layer for POMs in the synthesized solar cells [10,25]. Additionally, in these cells, the dye is attached to metal oxides through covalent-coordination bonds. In two recent works, Wang and coworkers have been synthesized a POM-TiO_2 composite and use this composite in working electrode [13]. In the other work, Li made Rh-substituted POM-TiO_2 composite and utilized it in DSC [26]. It goes without saying that most of these systems suffered from many problems and low efficiency, which should be solved in new designed DSC systems.

Herein, for overcoming these problems and achieving a novel method for synthesis of DSC based on POMs, a new hybrid system in which there is no under-layer was designed and an organic sensitizer was attached covalently to the POM in working electrode. In this system we used $[SiW_{11}O_{39}]^{8-}$ as a semiconductor instead of TiO_2 in the working electrode. An ordered thin film structure of Hybrid-POM with intrinsic high surface area could be easily fabricated by conventional printing methods. In order to attaching the dye to the POM through the net covalent bond, we made a pendant amine group at the end of the POM with attaching the (3-aminopropyl)triethoxysilane (APTES) at the vacant position of the lacunary-POM. Making the amide bond between the functionalized POM and the carboxylic group of the D35 dye was our devised path for attaching the dye to metal oxide with just covalent bond.

2. Experimental details

2.1 Synthesis and fabrication of D35@Hybrid-POM electrode

2.1.1 $[SiW_{11}O_{39}]$ thin film

For preparing the working electrode, first, the $[SiW_{11}O_{39}]^{8-}$ was synthesized according to the literature [27]. Then appropriate paste of POM using terpineol, ethanol and ethyl cellulose was made with previous reported procedure [22]. In the next step, this paste and Doctor-blade coating method was used for deposition of POM layer on the Fluorine-doped tin oxide (FTO) glass substrates (Pilkington, TEC15) which, were cleaned in an ultrasonic bath using (in order) detergent, water, and ethanol. The film thickness was evaluated by Dektak profilometer and cross section SEM image (Figure S1 in supporting information file) (about 6.4 μm).

2.1.2 $[SiW_{11}O_{39}(Si(CH_2)_3NH_2)_2O]$ (Hybrid-POM)

In this part, for functionalizing the POM we used (3-aminopropyl)triethoxysilane (APTES) to put pendant amine group at the end of POM. For this aim, 7 mg of $[SiW_{11}O_{39}]$ which is layered on the glass, treated with 30 μl of APTES in acetonitrile and then added 500 ml of HCL 2.4 M quickly after that. After 5 h of running the reaction in 0°C, the product can be departed from the reaction mixture. The FT-IR spectrum clearly showed the desired product. IR (KBr, cm^{-1}): 3448 (m), 2961 (s), 2934 (s), 2872 (s), 1482 (m), 1381 (m), 1153 (w), 1045 (s), 1010 (m), 965 (vs), 906 (vs), 807 (vs), 752 (s), 532 (m).

2.1.3 $[SiW_{11}O_{39}(Si(CH_2)_3NHCOC_{53}H_{57}N_2O_4S)_2O]$ (D35@Hybrid-POM)

In the final part of working electrode preparation, a triarylamine based organic dye with full name of (E)-3-(5-(4-(bis(20,40-dibutoxybiphenyl-4-yl)amino)phenyl)thiophen-2-yl)-2-cyanoacrylic acid (D35), which was prepared according to the published procedure [28], was attached to the POM through amide covalent bond. In this regard, 0.0002 mmol of D35 dye was added to the solution of 2-ethoxy-1-ethoxycarbonyl-1,2-dihydroquinoline (EEDQ) (0.0003 mmol) in refluxing acetonitrile. After stirring for 10 min, the functionalized layered POM was put in the reaction mixture and stayed overnight under reflux. The existence of amide bond in the FT-IR spectrum demonstrates the success of our desired conjugation. IR (KBr, cm^{-1}): 3327 (m), 2961 (s), 2932 (s), 2872 (s), 1626 (s), 1525 (m), 1482 (s), 1380 (m), 1150 (m), 1042 (m), 1006 (m), 967 (vs), 910 (vs), 791 (vs), 732 (s), 534 (s).

2.2 Fabrication of mesoporous TiO_2 electrodes

A mesoporous titania working electrode with and without thin layer of titania blocking layer was fabricated. The titania sol was prepared (for titania blocking layer (TBL)) using a previously reported procedure [29,30]. For preparing of working electrode, FTO glass substrates (Pilkington, TEC15) were also cleaned in an ultrasonic bath. The conducting glass substrates were coated in a dipping–withdrawing manner (withdrawing speed: 0.1 mm/s) (one layers) with titanium sol and preheated in 105 °C for 10 min. Mesoporous TiO_2 films were prepared with an area of 0.25 cm^2 by Doctor-blade from colloidal TiO_2 paste (Dyesol DSL 30 NRD-T) (two times) and sintered. The temperature gradient program had four levels at 180 (10 min), 320 (10 min), 390 (10 min), and 500 °C (60 min). Thickness of the layers was checked by Dektak profilometer (about 7 μm). After the sintering, when the temperature came down to 90 °C, the electrode was immersed in a dye bath containing 0.2 mM D35 in ethanol for 24 hr. Then the film was rinsed in ethanol to remove excess dyes.

2.3 Dye sensitized solar cell fabrication

Solar cells were assembled, using a 30 μm thick thermoplastic

Surlyn frame, with a platinized counter electrode (TEC8), which was prepared by spin-coating (10 µL cm^{-2}) 4.8 mM H_2PtCl_6 solution in ethanol on the glass substrate followed by heating in air at 400 °C for 30 min. A electrolyte solutions consisted of 0.22 M $[Co(bpy)_3](PF_6)_2$, 0.033 M $[Co(bpy)_3](PF_6)_3$, 0.1 M $LiClO_4$, and 0.2 M 4-*tert*-butylpyridine (TBP) in acetonitrile was then introduced through two holes predrilled in the counter electrode, and the cell was sealed with thermoplastic Surlyn covers and a glass coverslip.

2.4 Characterization methods

Powder X-ray diffraction (XRD) patterns of the samples were recorded on a Bruker, D8 ADVANCE, Germany, Wavelength: 1.5406 Å (Cu Kα), Voltage: 40 kV, Current: 40 mA in the 2θ range from 4 to 80. Infrared (IR) spectra were collected on a FT Infrared spectrometer, JASCO, FT/IR-6300 (400-4000 cm^{-1}), Japan. UV-vis diffuse reflectance spectra (UV-vis/DRS) were recorded on a UV-vis spectrophotometer, JASCO, V-670 (190-2700 nm), Japan using $BaSO_4$ as a reference. Current-voltage (I-V) and voltage-decay characteristics were measured using a home-made multi-functional potentiostat instrument and solar simulator giving light with AM1.5G spectral distribution, which was calibrated using a certified reference solar cell (Fraunhofer ISE) to an intensity 1000 W m^{-2}. A black mask with an aperture slightly larger (0.6 × 0.6 cm^2) than the active area of the solar cell (0.5 × 0.5 cm^2) was applied on top of the cell to avoid significant additional contribution from light falling on the device outside the active area. Incident photon to current conversion efficiency (IPCE) spectra were recorded using a computer-controlled setup consisting of a xenon light source (Nikon Xenon XE High Intensity Light Lamp), a monochromator (Spectral Products CM110 Compact 1/8 Meter), and a potentiostat (model BHP 2061-C, Behpajooh, Iran), calibrated using a certified reference solar cell (Fraunhofer ISE).

3. Results and discussion

3.1 Synthesis of D35@Hybrid-POM

In order to make an efficient connection between the dye and the working electrode (POM), making a covalent bond between POM and D35 as a dye molecule was designed. In this regard, first a layer of $[SiW_{11}O_{39}]^{8-}$ was made on the FTO glass. In the next step, for making an appropriate linker to attach the D35 to the POM, (3-aminopropyl)triethoxysilane was treated with POM to prepare an amine pendant group on the POM. Then, the D35 dye was attached to this functionalized POM through an amide bond. Comparing the FT-IR of the Hybrid-POM and the D35@Hybrid-POM clearly showed that the peak in 1626 cm^{-1} is a proof for formation of an amide bond (Figure 1). Additionally, existence the characteristic peaks of the POM in the hybrid product spectra, which correspond to the Si-O, W=O and W-O-W bonds, obviously demonstrates that POM structure has been remained intact during this synthesis.

3.2 Characterization of Hybrid-POM thin film

The XRD pattern of the Hybrid-POM thin film is shown in Figure 2a. The dominant peak at 7.5 degree presents the (111) plane of Keggin crystalline phase of POM. The powder XRD pattern of Hybrid-POM is compared to the simulated pattern using the data set obtained by single-crystal XRD analysis of $K_{10}A$-α-$[SiW_9O_{34}]\cdot 24H_2O$ (Figure 2b) [31]. It is suggested that the grains in the Hybrid-POM thin film have a strongly preferential orientation along (111) direction in the working electrode in compare with other SiW_xO_yPOMs XRD patterns in the powder form [32,33].

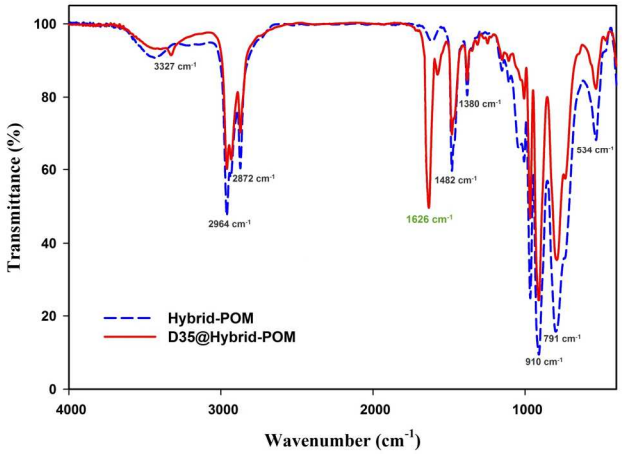

Figure 1: FT-IR spectra of the Hybrid-POM thin film before and after loading of D35**.**

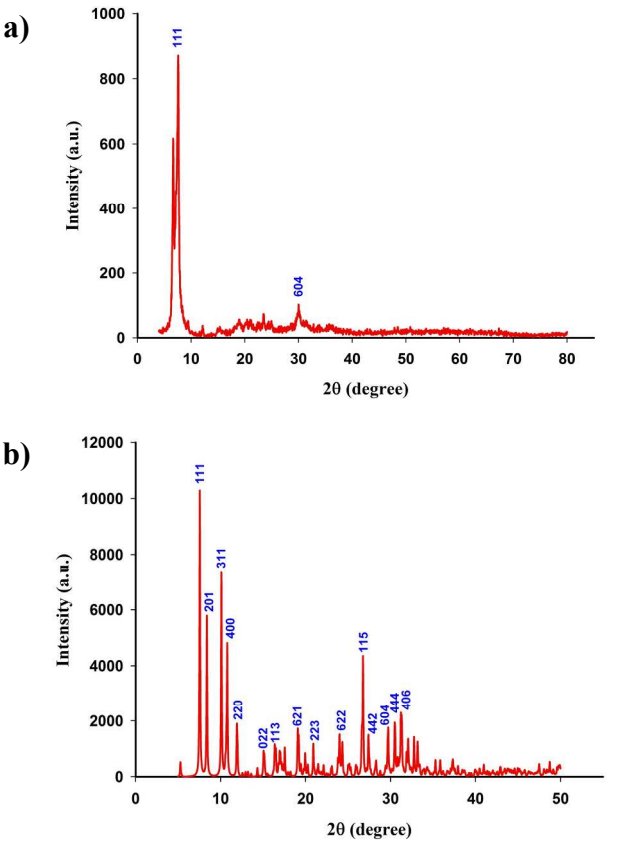

Figure 2: XRD patterns of the Hybrid-POM thin film (a) and simulated pattern using the data set obtained by single-crystal XRD analysis of K10A-α-$[SiW_9O_{34}]$•$24H_2O$ [31] (b).

The UV-vis reflection spectrum of the Hybrid-POM thin film is measured before and after loading of D35 and shown in Figure 3a. A strong reflection is presented in the range of 290-485 nm with maximum reflection values of 87% that is related to POM absorption in 275 nm. After loading of D35, an extra reflection is took place in 510-700 nm, which is related to the broad absorption of D35 in 530 nm.

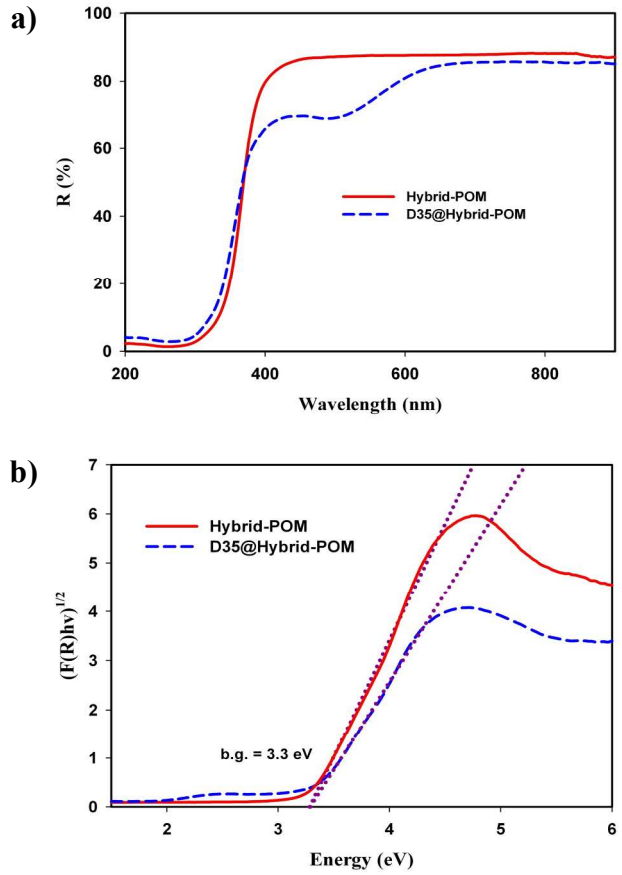

Figure 3: UV-vis reflection spectra of the Hybrid-POM thin film before and after loading of D35 (a). Transformed UV-vis DRS spectra in the Kubelka-Munk equation (b).

The optical absorption coefficient (α) is calculated using reflectance data according to the Kubelka-Munk equation, $F(R) = \alpha = (1-R)^2/2R$, where R is the percentage of reflected light [34]. The incident photon energy (hν) and the optical band gap energy (E_g) are related to the transformed Kubelka-Munk function, $[F(R)h\nu]^p = A(h\nu - E_g)$, where E_g is the band gap energy, A is the constant that depends on transition probability and p is the power index that is related to the optical absorption process. Theoretically p equals to 1/2 or 2 for an indirect or direct allowed transition, respectively. Band-gap energies of both Hybrid-POM and D35@Hybrid-POM films are determined to be 3.3 eV based on the indirect transition (Figure 3b).

From the interference pattern, the refractive index n_f can be calculated using Equation 1: [35]

$$n_f = p\frac{\gamma_1\gamma_2}{2d(\gamma_1-\gamma_2)} \quad (1)$$

Where λ_1 and λ_2 are the wavelength of two interference maxima and p is the number of maxima between λ_1 and λ_2 plus one. The refractive index is determined to be 1.35, which is lower than that of bulk standard polyoxometalates refractive index ($n_s \sim 2$) [36]. By use of simpler approach in Lorentz-Lorenz formula, the refractive index of the film is the volume fraction weighted sum of the refractive indices of polyoxometalates and air Equation 2:

$$n_f = V_s n_s + (1 - V_s)n_{air} \quad (2)$$

Using this formula, V_s is calculated to be 0.35 and the porosity 0.65. These values are in good agreement with high porosity film structures.

Surface structure and film thickness of the Hybrid-POM film are evaluated by FE-SEM and TEM analysis. High porosity structure of the film surface with average hole diameter as 10 nm is presented in FE-SEM image from the surface of Hybrid-POM film (Figure S1-a). Cross section FE-SEM image of the film layer show thickness of 6.38 μm. Furthermore, TEM image from Hybrid-POM nanoparticles show high ordered arrangement of the polyoxometalate clusters toward 111 crystalline directions (Figure S1-c).

The dye coverage based on mol per square centimeter was determined according to optical absorption data of dyes films (figure S2). Using the Standard formulas, we obtained dye coverage (Γ) of 2.5×10^{-7} (mol cm^{-2}) for coverage of D35 on the polyoxometalate surface. Additionally, having the dye coverage value for D35, we can calculate the Langmuir adsorption isotherm (Γ_{max}) to 2.6×10^{-7} for a 6.4 μm thick Polyoxometalate film. Amide covalent bonding of D35 molecules on the Hybrid-POM led to increase of dye coverage compare to mp-TiO_2 [37].

Through the BET analysis we obtained the total pore volume of 0.52 cm^3/g and porosity of 71%. BET results are shown enhancement of Hybrid-POM film porosity compare to mp-TiO_2 film [37]. Using surface area of 1033.5 cm^2, area occupied by a D35 molecule on polyoxometalates: $1033.5 \times 10^{14} / (2.6 \times 10^{-7} \times 6.023 \times 10^{23}) = 0.66$ nm^2.

3.3 Photovoltaic results

D35@Hybrid-POM thin film was selected to use as a working electrode in dye-sensitized solar cells not only for proper band-gap energy but also Keggin crystalline structure could improve the electron mobility inside the layer. Furthermore, (3-aminopropyl)triethoxysilane linker can provide an efficient terminal for covalent bonding of the D35 on the POM layer.

Photovoltaic parameters of the devices are evaluated by I-V measurement technique. Statistical variation box plots of the photovoltaic parameters for Hybrid-POM-based DSCs are presented in Figure 4. Furthermore, these parameters are compared to the titania-based DSCs with blocking layer (mp-TiO_2 with TBL) and without any blocking layer (mp-TiO_2 without BL). The power conversion efficiency (η) was derived from the equation $\eta = J_{sc}V_{oc}FF/I_0$, where J_{sc} is the short-circuit current density, V_{oc} is the open-circuit voltage, FF is the fill factor, and I_0 is the photon flux illuminating the solar cells. The DSC parameters of selected cells are calculated and listed in Table 1.

By using of polyoxometalate structure, photovoltage values of the

cells are improved to 900 mV which is about 100 mV higher than mp-TiO_2-based cells. Statistical correlation between Voc values shows high variation for mp-TiO_2 samples without blocking layer. Comparison of the Jsc values show promising enhancement of photocurrent in the Hybrid-POM device about 13 mA/cm^2 that is higher than other reported values of D35-based DSCs. On the other hand, fill factor values of the hybrid-POM devices are improved to 70%. Totally, overall efficiencies of the Hybrid-POM devices are improved to 8% which is two-fold higher than mp-TiO_2-based devices.

Incident photon to current conversion efficiency (IPCE) spectra were recorded for DSCs fabricated by D35@Hybrid-POM and mesoporous titania with blocking layer, see Figure 5. The IPCE for the Hybrie-POM-based DSC show higher values between 350 nm to 650 nm (absorption range of D35) in compare with mp-TiO_2-based DSC. A maximum IPCE of about 91% was found for DSCs employing Hybrid-POM which is about 30% higher than the DSC with mesoporous titania layer (61%). High values of IPCE in Hybrid-POM-based DSC could be attribute to not only faster electron injection between D35 and POM structure via pure covalent band, but also higher electron mobility (electron diffusion) inside Keggin structure of the POM.

The voltage, V, is difference between the Nernstian potential of the solution, $E(R^+/R)$, and the quasi-Fermi level, $E_{F/q}$, (i.e. potential of the semiconductor) at the contacting electrode. At open circuit, the photocurrent density is exactly offset by recombination, U_{rec}. Recombination is generally used to refer to electron transfer from the semiconductor to the oxidized dye and the oxidized form of the redox shuttle [38,39]. The largest increasing in V_{oc} could be realized by making the solution potential more positive and/or increasing in the quasi-Fermi energy of the semiconductor material. The open circuit photovoltage is thus highly sensitive to the properties of the redox couple and electronic states of the semiconductor material. In the present work, all the DSCs were fabricated with similar electrolyte medium, thus higher values of the V_{oc} could be attribute to higher energy of the quasi-Fermi level of D35@Hybrid-POM, in comparison with mesoporous TiO_2. Furthermore, crystalline structure of photoanode layer can directly affect on V_{oc} values. Jadhav, et al. are shown that photoelectric performance is strongly dependent on combined effect of V_{oc} and J_{sc} which shows the characteristic change with structure texture morphology as well as pore size and specific surface area of fabricated electrode [40].

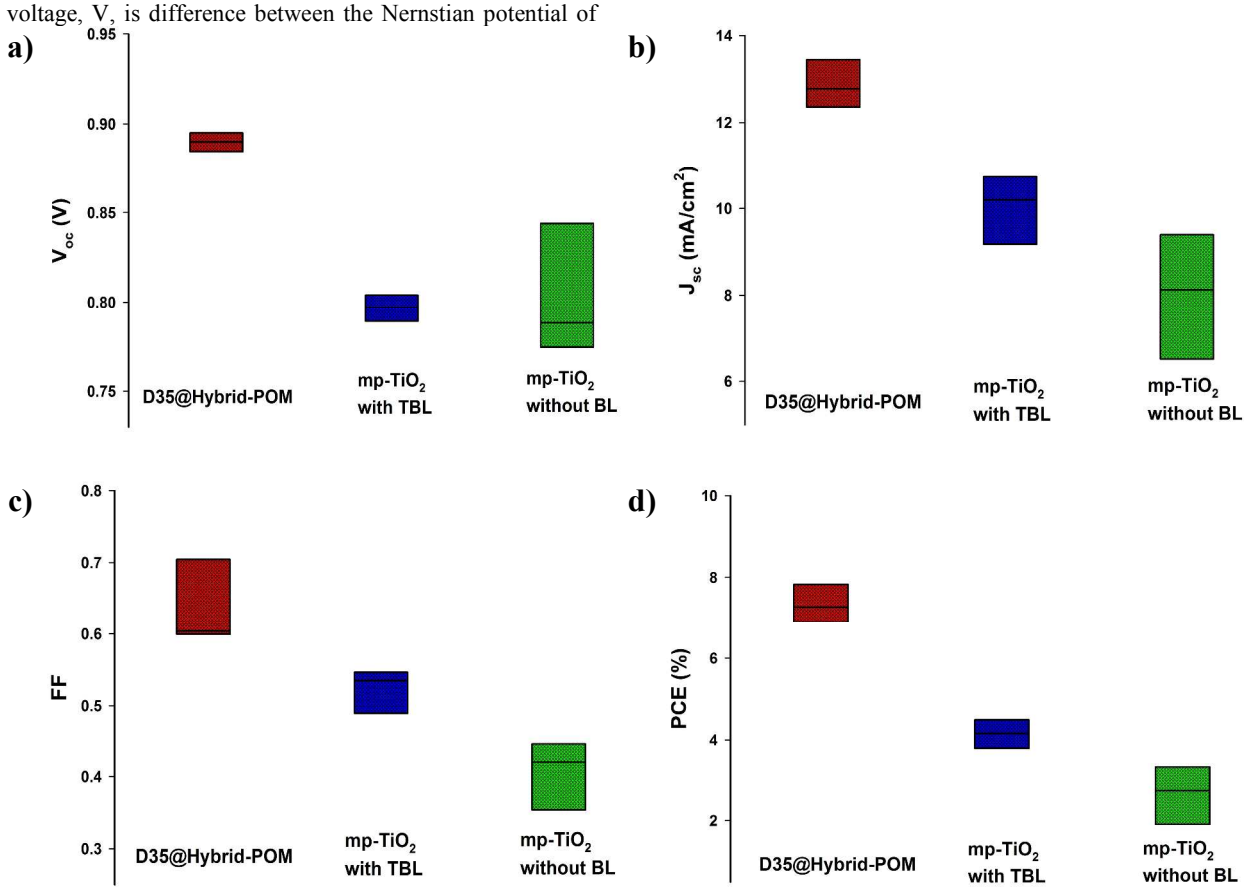

Figure 4: Statistical variation box plots of the photovoltaic parameters for Hybrid-POM, mesoporous TiO_2 with blocking layer and mesoporous TiO_2 without blocking layer. Effect of V_{oc} (a), J_{sc} (b), FF (c) and overall efficiency (d).

Table 1: Dye-sensitized solar cells parameters from J-V measurement of DSCs with D35@Hybrid-POM, Mesoporous titania with and without blocking layer under AM1.5G irradiation.

Efficiency (%)	V_{oc} (V)	J_{sc} (mAcm^{-2})	FF	Sample
8.02	0.899	12.78	0.697	D35@Hybrid-POM
4.63	0.787	10.98	0.536	mp-TiO_2 with TBL
3.56	0.844	9.02	0.468	mp-TiO_2 without BL

The maximum fill factor is strictly a function of the diode quality factor, γ, and the V_{oc} [41]. There are different processes, which can cause the apparent diode quality factor to exceed the ideal value of 1, including surface state mediated recombination. Direct electron transfer from the semiconductor substrate to the electrolyte (shunting) can impact the fill factor, especially in cases where outer-sphere redox shuttles are used [39]; however this can be overcome through use of a blocking layer [42,43]. The actual fill factor is also attenuated in the cell by any uncompensated series resistance (R_s). Including γ and R_s, the J–V characteristics can be described in terms of the diode equation written as:

$$J = J_{sc} - q\tau_0^{-1}\zeta n_0(\exp\left(\frac{-q(V+IR_s)}{\gamma kT}\right) - 1) \quad (3)$$

High fill factor values of the cell with D35@Hybrid-POM could be attribute to stepping down of recombination reaction between POM surface and electrolyte. Keggin-type structure of Hybrid-POM provides a strong electron accepter cluster which can easily accept the photoelectron in the vacant *d* orbitals of tungsten metal core. Thus, injected electrons could quickly diffuse into space charge double layer of Hybrid-POM. Thereupon, the amounts of the injected electrons on the interfacial (electrode/electrolyte) double layer will be reduced, and caused to improve the shunt resistance of electron recombination process at the uncoated surface of the semiconductor. Furthermore, very high photocurrent values that collected from the cell with D35@Hybrid-POM, is also other promising result of cluster-type structure of the photoanode layer. $[SiW_{11}O_{39}]^{8-}$ clusters with diameters about 1-1.5 nm are strongly attached together [44] and this assembling of the clusters led to increase of the trap states and promising improvement of electron diffusion into semiconductor layer. On the other hand, very strong attachment of the D35 dye with (3-aminopropyl)triethoxysilane linker by covalent bond in line with the hole site of the lacunary-POM, can improve the rate of electron injection of the photoexcited electron to conduction bond of Hybrid-POM and led to increase of photocurrent.

By open-circuit voltage decay technique we could have deeper knowledge in dye regeneration and recombination process in DSCs [45,46]. Voltage decay curves of DSCs with D35@Hybrid-POM, and mesoporous titania with TBL and without BL are shown in Figure 6a. The DSC with D35@Hybrid-POM layer in photoanode, shows very slow decay of open-circuit voltage in compare with two other cells. Transients (V(t)) electron lifetimes in the DSCs are calculated and shown in Figure 6b. The inset in Figure 6b shows that the DSC with D35@Hybrid-POM have higher τ_e values from 0.5 to 3.2 second in the voltage range of 0.50 to 0.10 V but the electron lifetimes of the DSCs with titania are below 0.3 second.

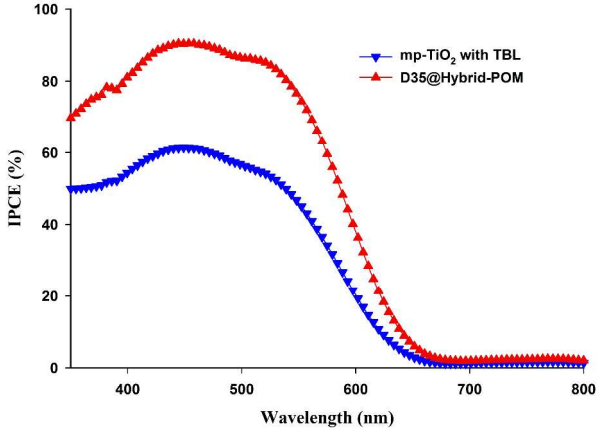

Figure 5: Spectra of incident photon to current efficiency (IPCE) for DSCs based on D35@Hybrid-POM and mesoporous titania with TBL working electrodes.

Wang et al. are presented the relation between electron lifetimes with electron transport process in a polyoxometalate-TiO_2 composite by open-circuit voltage decay and electrochemical impedance spectroscopy [13]. High electron lifetimes in the DSC with Hybrid-POM layer could directly related to higher electron transport process inside the photoanode layer. The effective recombination order (β) is calculated using a model, including trapping effects and are presented in Figure 6c [47]. The β values of the D35@Hybrid-POM and titania without blocking layer cells are approximately constant of about 1.2 in all the voltage ranges which show a constant mechanism of the electron transfer. Voltage decay and electron lifetime results of the DSC with D35@Hybrid-POM are in good agreement with J-V measurement results, which show a very slow recombination reaction at the surface of POM clusters.

The results from electrochemical impedance spectroscopy analysis of the DSCs (shown in Fig. S3) are consistent with the above analysis. Nyquist plots of the DSCs containing mp-TiO_2 and Hybrid-POM are evaluated in different voltages. The distributed interfacial charge transfer resistance (R_{ct}) is strongly affected by changing of the photoanode layer. R_{ct} is significantly increases by changing of mp-TiO_2 to polyoxometalate. This confirms that the interfacial electron transfer inside the POM layer is very high compare to electron diffusion in the

mesoporous titania layer. Unoccupied *d* orbitals of tungsten can prepare a sufficient direction for electron diffusion between POM clusters and increase of the photogenerated charge collection in the device. Furthermore, strongly preferential orientation along (111) direction could reduce the electron transition dead-ends compare to random orientation of mesoporous anatase TiO_2 grains.

4. Conclusions

In the present work, a new efficient dye-sensitized solar cell using a pure thin film layer of functionalized Keggin-type POM as photoanode in a cobalt-complex based electrolyte medium has been reported. (3-Aminopropyl)triethoxysilane linker provides an efficient terminal group for covalent amide binding of the D35 on the POM surface. Furthermore, crystalline structure of the Hybrid-POM led to increasing in the electron life-time and decreasing in the recombination of the electron with redox mediator on the surface. This assembled structure not only led to promising improvement of the photocurrent (J_{sc}) and IPCE values, but also increased all photovoltaic parameters and overall efficiency.

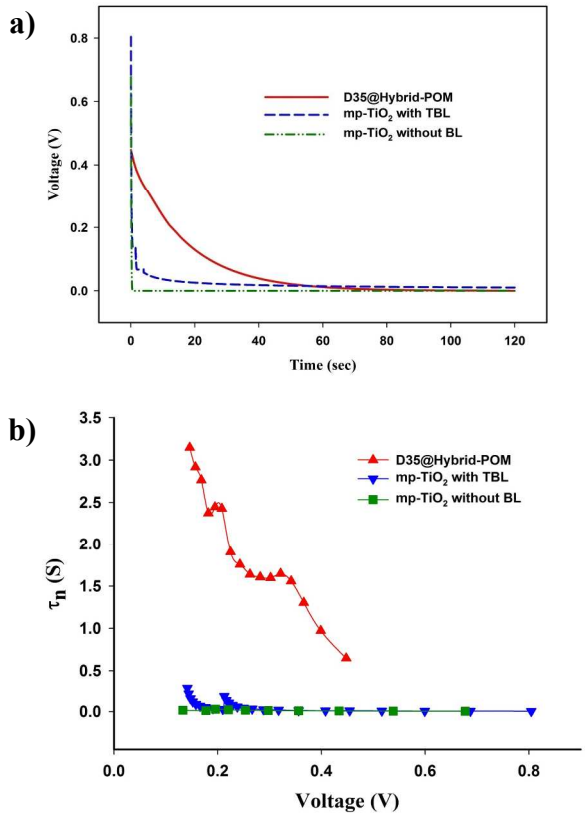

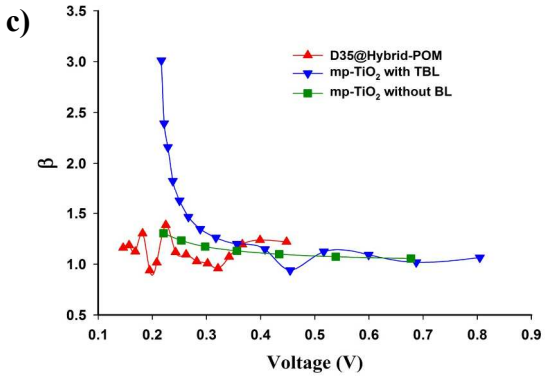

Figure 6: Experimental V_{oc} decay results of the DSCs with D35@Hybrid-POM and mesoporous titania working electrodes. a) Measured $V_{oc}(t)$. b) The electron lifetime as a function of V_{oc}. c) Recombination β-parameter (effective recombination order) as a function of V_{oc}.

Acknowledgments

The authors wish to thank the University of Isfahan for financially supporting of this work.

References

[1] M. T. Pope and A. Müller, *Angew.Chem., Int. Ed.*, 1991, **30**, 34.
[2] M. T. Pope and A. Müller, *Polyoxometalate Chemistry From Topology via Self-Assembly to Applications*, *Kluwer Academic Publishers, Dordrecht, Netherlands,* 2001.
[3] H. Park and W. Choi, *J. Phys. Chem. B,* 2003, **107**, 3885.
[4] Z. X. Sun, L. Xu, W. H. Guo, B. B. Xu, S. P. Liu and F. Y. Li, *J. Phys. Chem. C,* 2010, **114**, 5211.
[5] N.V. Izarova, M.T. Pope and U. Kortz, *Angew. Chem. Int. Ed.,* 2012, **51**, 9492.
[6] X.P. Zheng, Y. Lu, H. Zhang, Z.M. Zhang and E.B. Wang, *Inorg. Chem. Commun.,* 2013, **33**, 29.
[7] Z.Wang, Y.Ma, R. Zhang, A. Peng, Q. Liao, Z. Cao, H. Fu and J. Yao, *Adv. Mater.,* 2009, **21**, 1737.
[8] L. Wang, L. Xu, Z. Mu, C. Wang and Z. Sun, *J.Mater. Chem.,* 2012, **22**, 23627.
[9] N. Fu and G. Lu, *Chem. Commun.,* 2009, 3591.
[10] A. Dolbecq, E. Dumas, C.R. Mayer and P. Mialane, *Chem. Rev.,* 2010, **110**, 6009.
[11] (a) T. Tachikawa, S. Tojo, M. Fujitsuka and T. Majima, *Chem. Eur. J.,* 2006, **12**, 3124., (b) D. Karimian, B. Yadollahi and V. Mirkhani, *Dalton Trans*., 2015, **44**, 1709.
[12] X.-J. Sang, J.-S. Li,W.-L. Chen and E.-B.Wang, *Mater. Lett.,* 2012, **87**, 39.
[13] S.-M. Wang, L. Liu, W.-L. Chen, E.-B. Wang and Z.-M. Su, *Dalton Trans.,* 2013, **42**, 2691.
[14] J.-S. Li, X.-J. Sang, W.L. Chen, C. Qin, S.-M. Wang, Z.-M. Su and E.-B.Wang, *Eur. J. Inorg. Chem.,* 2013, **2013**, 1951.
[15] B. O'Regan and M. Grätzel, *Nature,* 1991, **353**, 737.
[16] A. Hagfeldt, G. Boschloo, L. Sun, L. Kloo and H. Pettersson, *Chem. Rev.*, 2010, **110**, 6595.
[17] Q. Zhang, E. Uchaker, S. L. Candelaria, G. Cao, *Chem. Soc. Rev*., 2013, **42**, 3127.
[18] M. Nazeeruddin, A. Kay, I. Rodicio, R. Humphry-Baker, E.

Muller, P. Liska, N. Vlachopoulos and M. Grätzel, *J. Am. Chem. Soc.,* 1993, 115, 6382.
[19] S. M. Feldt, E. A. Gibson, E. Gabrielsson, L. Sun, G. Boschloo and A. Hagfeldt, *J. Am. Chem. Soc*., 2010, **132**, 16714.
[20] S. Zhang, X. Yang, Y. Numata, L. Han, *Energy Environ. Sci*., 2013, **6**, 1443.
[21] S. A. Sapp, C. M. Elliott, C. Contado, S. Caramori, C. A. Bignozzi, *J. Am. Chem. Soc*., 2002, **124**, 11215.
[22] M. H. Habibi, M. Mikhak, M. Zendehdel and M. Habibi, *Int. J. Electrochem. Sci.,* 2012, **7**, 6787.
[23] M. H. Habibi, A. H. Habibi, M. Zendehdel and M. Habibi, *Spectrochim. Acta A*, 2013, **110**, 226.
[24] M. H. Habibi, E. Askari, M. Habibi and M. Zendehdel, *Spectrochim. Acta A*, 2013, **104**, 197.
[25] G. Jin, S.-M. Wang, W.-L. Chen, C. Qin, Z.-M. Su and E.-B. Wang, *J. Mater. Chem. A,* 2013, **1**, 6727.
[26] J.-S. Li, X.-J. Sang, W.-L. Chen, L.-C. Zhang, Z.-M. Sua, C. Qin and E.-B. Wang, *Inorg. Chem. Commun.,* 2013, **38**, 78.
[27] P. Souchay, *Polyanions et Polycations; Gauthier-Villars: Paris,* 1963.
[28] D. P. Hagberg, X. Jiang, E. Gabrielsson, M. Linder, T. Marinado, T. Brinck, A. Hagfeldt and L. Sun, *J. Mater. Chem.,* 2009, **19**, 7232.
[29] M. H. Habibi and M. Zendehdel, *Curr. Nanosci.*, 2010, **6**, 642.
[30] M.H. Habibi and M. Zendehdel, *J. Inorg. Organomet. Polym*., 2011, **21**, 634.
[31] N. Laronze , J. Marrot and G. Hervé, *Inorg. Chem.*, 2003, **42**, 5857.
[32] M. Sadakane, Y. Limuro, D. Tsukuma, B. S. Bassil, M. H. Dickman, U. Kortz, Y. Zhang, S. Ye and W.Ueda, *Dalton Trans.,* 2008, **47**, 6692.
[33] J. Gao, S. Cao, Q. Tay, Y, Liu, L. Yu, K. Ye, P. C. S. Mun, Y. Li, G. Rakesh, S. C. J. Loo, Z. Chen, Y. Zhao, C. Xue, Q. Zhang, *Sci. Rep.* 2013, **3**, 1853.
[34] H. Lin, C. P. Huang, W. Li, C. Ni, S. I. Shah and Y.-H. Tseng, *Appl. Catal. B.,* 2006, **68**, 1.
[35] G. Boschloo and D. Fitzmaurice, *J. Phys. Chem. B.*, 1999, **103**, 2228.
[36] A. V. Sankarraj, *Electrocatalytic and Antibacterial Application of Sandwich type Polyoxometalates*, *Auburn University*, 2008, p. 89.
[37] M. Pazoki, P. W. Lohse, N. Taghavinia, A. Hagfeldt and G. Boschloo, *Phys. Chem. Chem. Phys*., 2014, **16**, 8503.
[38] M. Nasr-Esfahani, M. Zendehdel, N. YaghoobiNia, B. Jafari and M. KhosraviBabadi, *RSC Adv.,* 2014, **4**, 15961.
[39] N. YaghoobiNia, P. Farahani, H. Sabzyan, M. Zendehdel and M. Oftadeh, *Phys. Chem. Chem. Phys*., 2014, **16**, 11481.
[40] N. A. Jadhav, P. K. Singh, H- W Rhee, S. P. Pandey and B. Bhattacharya., *Int. J. Electrochem. Sci*., 2014, **9**, 5377.
[41] T. W. Hamann, J. W. Ondersma, *Energy Environ. Sci*., 2011, **4**, 370.
[42] B. M. Klahr, T. W. Hamann, *J. Phys. Chem. C*, 2009, **113**, 14040.
[43] T. W. Hamann, O. K. Farha, J. T. Hupp, *J. Phys. Chem. C*, 2008, **112**, 19756.
[44] Y. Wang and I. A. Weinstock, *Chem. Soc. Rev.,* 2012, **41**, 7479.
[45] M. H. Habibi, B. Karimi, M. Zendehdel, M. Habibi, *J. Ind. Eng. Chem.* 2014, **20**, 1462.
[46] M. H. Habibi, B. Karimi, M. Zendehdel, M. Habibi, *Spectrochim. Acta part A,* 2013, **116**, 374.
[47] A. Zaban, M. Greenshtein, J. Bisquert, *ChemPhysChem,* 2003, **4**, 859.

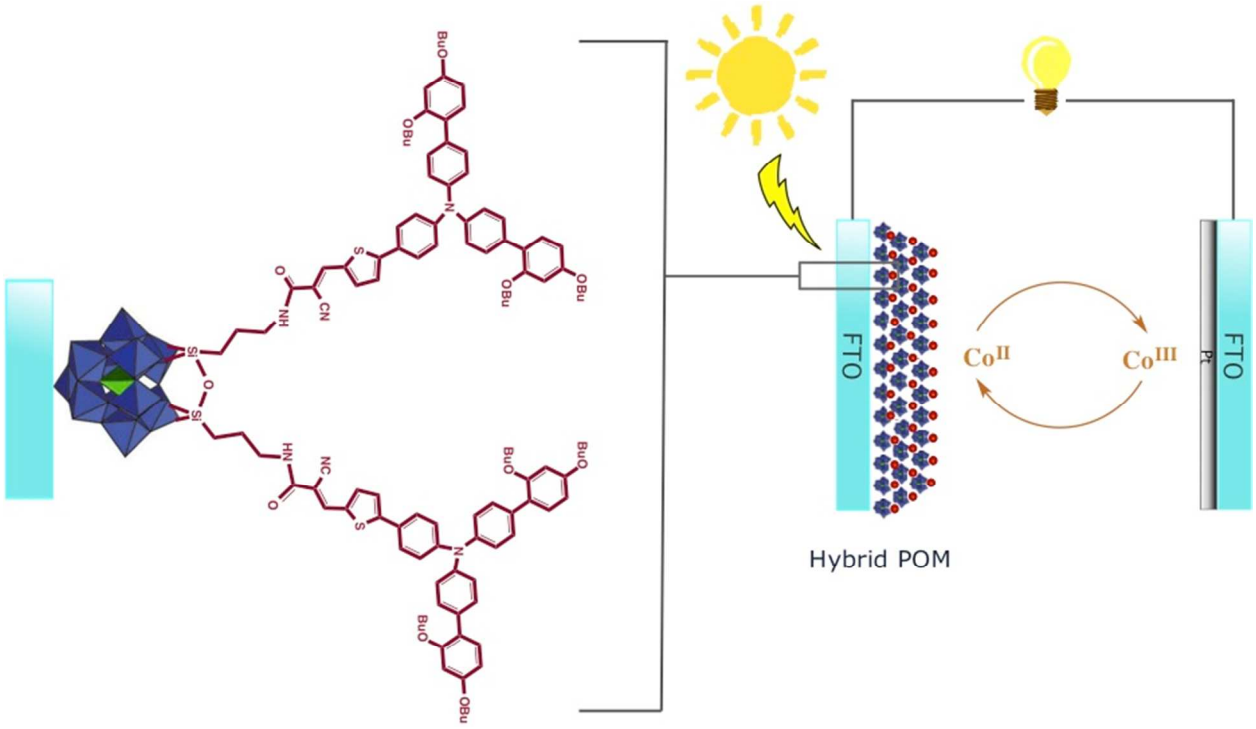

Graphical Abstract